Journal of Dentistry 90 (2019) 103211

Contents lists available at ScienceDirect

Journal of Dentistry

journal homepage: www.elsevier.com/locate/jdent

Remineralizing potential of dental composites containing silanized silica-hydroxyapatite (Si-HAp) nanoporous particles charged with sodium fluoride (NaF)

Dirciane Perpétuo Reis[a], Jaime Dutra Noronha Filho[a], André Linhares Rossi[b], Aline de Almeida Neves[c], Maristela Barbosa Portela[d], Eduardo Moreira da Silva[a,*]

[a] Analitical Laboratory of Restorative Biomaterials – LABiom-R, School of Dentistry, Universidade Federal Fluminense, Niterói, Rio de Janeiro, Brazil
[b] Brazilian Center for Research in Physics, Rio de Janeiro, Brazil
[c] Department of Pediatric Dentistry and Orthodontics, School of Dentistry, Universidade Federal do Rio de Janeiro, Rio de Janeiro, Brazil
[d] Odontopediatric Division, School of Dentistry, Universidade Federal Fluminense, Niterói, Rio de Janeiro, Brazil

ARTICLE INFO

Keywords:
Dental composite
Nanoporousparticles
Hydroxyapatite
NaF
Silanization
Enamel remineralization

ABSTRACT

Objectives: To synthesize and evaluate the enamel remineralizing potential of dental composites containing silanized silica-hydroxyapatite (Si-HAp) nanoporous particles charged with sodium fluoride (NaF).
Methods: Si-HAp particles were synthesized using a solid-state method. Dental composites were prepared by incorporating 70 wt.% of Si-HAp particles into a 70/30 wt.% Bis-GMA/TEGDMA organic matrix. Four dental composites were produced: SilF, Sil, F, and NT (nontreated). For SilF and F, Si-HAp particles were previously treated with 10% NaF (F). Afterwards, SilF and Sil composites had their particles silanized (Sil) with α-methacryloxypropyl-1-trimethoxysilane (α-MPS). The remineralizing potential was evaluated in caries-like enamel lesions induced by*S. mutans* biofilm for seven days and after pH-cycling for fifteen days using X-ray microtomography (micro-CT). Z350 was used as a commercial control for remineralizing potential evaluation Degree of conversion (DC%), flexural strength (FS), and Knoop hardness (KHN) were characterized. Data were analyzed using one-way ANOVA and Tukey's HSD post-hoc test ($\alpha = 0.05$).
Results: F presented the highest enamel remineralizing potential, followed by SilF. Alternatively, Sil and NT were not capable of totally recovering the enamel mineral loss. NT showed the highest DC%, followed by Sil, F, and SilF. Sil and NT showed the highest FS when compared to SilF and F. No statistical significance in KHN was found among the composites.
Conclusions: Dental composites with Si-HAp nanoporous particles charged with NaF presented a remineralizing potential for human enamel. However, this ability underwent a subtle reduction after particle silanization.
Clinical significance: Si-HAp nanoporous particles charged with NaF may be an alternative for producing dental composites with an improved remineralizing potential for enamel affected by caries.

1. Introduction

Irrespective of the improvement in the dental clinical practice over the last decades, the development of recurrent caries at tooth-restoration interfaces still remains as one of the principal reasons for replacement of different kinds of restorations [1–4]. Based on this, one of the greatest challenges in the field of restorative dentistry involves the development of restorative biomaterials that have the ability of avoiding demineralization or promoting remineralization of hard dental tissues affected by caries [5,6]. Among existing strategies to this end, the development of resin composites with bioactive particles able to release high levels of Ca^{2+}, PO_4^{3-}, and F^-,which are capable of reinforcing the teeth against the action of organic acids produced by the oral biofilm, has been attempted [7–12].

The demineralization of the hard dental tissues occurs when cariogenic bacterias, e.g. *S. mutans*, metabolize carbohydrates through fermentation, thereby producing acids that lower the pH inside the oral biofilm [13]. However, if fluorides are available in the medium, the dissolution of tooth minerals is reduced because some Ca^{2+} and PO_4^{3-} lost as hydroxyapatite precursors returns to the enamel as the more

* Corresponding author at: Universidade Federal Fluminense/Faculdade de Odontologia - Rua Mário Santos Braga, nº 30 - Campus Valonguinho, Centro, Niterói, RJ, CEP 24040-110, Brazil.
E-mail address: em_silva@id.uff.br (E.M. da Silva).

https://doi.org/10.1016/j.jdent.2019.103211
Received 18 February 2019; Received in revised form 23 September 2019; Accepted 8 October 2019

acid-resistant fluoroapatite. Also, in the absence of carbohydrate intake, the oral pH rises and the fluorides present in the oral fluids enhance the remineralization of the enamel. It is clear that remineralization is a F^--dependent mechanism involving pH changes inside the oral cavity [14]. Thus, the development and the usage of composites capable of releasing high levels of Ca^{2+}, PO_4^{3-} and F^- might counterattack the development of caries at the tooth-restoration interfaces, while also inducing remineralization of the hard dental tissues exposed to bacterial acids [14,15].

During fabrication of dental composites, silanization of the inorganic particles is used to improve their interfacial chemical interaction with the organic matrix, which, in turn, may improve the composite mechanical properties [16]. Although there is scarce information about the influence of this process on the ion release capability of bioactive composites with different calcium phosphate complexes [17], its effect on enamel remineralization seems to be missing. Therefore, we evaluated the enamel remineralizing potential of dental composites containing silanized silica-hydroxyapatite (Si-HAp) nanoporous particles charged with sodium fluoride (NaF). The tested hypotheses were: 1) NaF-charged composites would better remineralize caries-like enamel lesions than non-NaF-charged composites; 2) particles silanization would not influence the remineralizing potential of the composite.

2. Materialandmethods

2.1. Production and characterization of Si-HAp nanoporous particles

Hydroxyapatite [$Ca_{10}(PO_4)_6(OH)_2$] was synthesized using a wet precipitation method and a theoretical ratio of ions $[Ca]^{+2}/[PO_4]^{-3} = 1.67$, according to the method described by Ellis et al [18]. Briefly, an aqueous solution of (NH4)2HPO4 was added dropwise to a solution of Ca(NO3)2 at 80 °C, pH = 11. After the addition, the mixture was stirred for 2.5 h at the same temperature. The precipitate was separated by filtration, repeatedly washed with deionized boiling water, and dried at 100 °C for 24 h.

Hydroxyapatite size distribution was analysed using the NanoSight LM10 system (Malvern Instruments Ltd., Worcestershire, UK). The viscosity of the suspension medium was 0.95 cP, and the testing temperature was 22 °C. Ten samples (n = 10) of the HAp powder were evaluated for 30 s, employing 30 frames per second, with a camera shutter of 1 ms. The software used for capturing and analysing the data was the NTA 2.3 Build 0025. The mean size determined by the NTA software corresponds to the arithmetic values of all the particles analyzed.

A mixture (50/50 wt.%) of 40 nm silica nanoparticles (Aerosil OX 50, Evonik, USA) and HAp were previously immersed in acetone p.a. and mixed for 20 min using a magnetic stirrer (Q261A11, Quimis, Rio de Janeiro, Brazil) to decrease agglomeration. Next, the particles were thermally sintered in an electric tubular furnace (FTE 1700 H - Fortelab, São Paulo, Brazil) at 900 °C for 15 min, with a heating rate of 20 °C / min. The sintered blocks were crushed for 30 min in a micronizing mill (Glen Creston – McCrone Micronising Mill. Londres, Reino Unido) to obtain nanoporous Si-HAp particles. The Si-HAp particles were characterized using field emission-transmission electron microscopy (FE-TEM) and the Multipoint Brunauer-Emmett-Teller (BET) method.

For TEM analysis, the Si-HAp particles were dissolved in acetone at room temperature and dripped over copper grids with an amorphous carbon film. Afterwards, the copper grids were inserted into a sample-holder and observed under FE-TEM. The microscopy (JEM-2100 F, JEOL Ltd., Japan) was handled at 200 kV, with 0.25 nm of point-to-point resolution.

The surface structure parameters of Si-HAp particles were calculated from the N_2 adsorption/desorption isotherms using an accelerated surface area and a porosimetry analyser (ASAP 2020, Micrometrics, GA, USA). The samples of Si-HAp particles were first degassed at 50 °C for 60 min under vacuum (4 μHg) and the temperature was raised to 240 °C until reaching the pressure of 4 μHg again. Isothermals were generated from 40 points of adsorption and 40 points of desorption. The Si-HAp particles specific area was calculated using the multipoint BET method and the pore volume by the Barrett-Joyner-Halenda (BJH) method.

Table 1
Composition of the dental composites.

Composite	Si-HAp fillers treament
SilF	Treatment of fillers with 10% NaF + silanization
Sil	Silanization
F	Treatament of fillers with 10% NaF
NT	No surface treatment

2.2. Synthesis of dental composites

Four dental composites were synthesized (Table 1). The organic matrix (40 wt.%) consisted of Bis-GMA and TEGDMA (Essthec, Inc. Essington, PA, USA) with a mass ratio of 70:30 wt.%. The reinforcing particles consisted of 60 wt.% of Si-HAp nanoporous particles. In two composites (SilF and F), the particles were immersed during 24 h in 10% NaF aqueous solution (pH = 6.5) and maintained for 7 days in a dryer at 40 °C (Q317 M, Quimis, Rio de Janeiro, Brazil). The sodium fluoride was diluted in deionized water and this solution was maintained for 30 min at 60 °C to avoid NaF precipitation [19]. Afterwards, the particles of SilF and Sil were silanized using α-methacryloxypropyl-1-trimethoxysilane (α-MPS). The silanization of the particles was carried out using the method described by Chen & Brauer [20]. The minimum amount of silane used to cover the particles (X) was calculated according to the following equation:

$$X = \left(\frac{A}{\omega}\right) f,$$

where A is the surface area of 1 g of the Si-HAp particles (BET of the Si-HAp particles $= 18\ m^2.g^{-1}$), ω is the surface area of coverage per g of silane (MPTS $= 2525\ m^2.g^{-1}$), [21] and f is the amount of Si-HAp particles (g). The Si-HAp particles, the silane, the solvent (cyclohexane, 100 mL) and n-propylamine (0.1 g) were stirred at room temperature for 30 min and then at 60 °C for 30 min in a magnetic stirrer (Q261A11 – Quimis, Rio de Janeiro, Brazil). Afterward, this mixture was placed in a rotary evaporator (G344B1 – Quimis, Rio de Janeiro, Brazil) at 60 °C to volatilize the solvent and the subproducts, until only the dry products remained. The resulting powder was heated at 90 °C for 1 h in the rotary evaporator to condensate the silane in the surface of the particles and dried at 50 °C for 48 h in a dryer (Q317M-22 – Quimis, Rio de Janeiro, Brazil).

Finally, camphorquinone (0.5 wt.%) and ethyl N, N-dimethyl- 4-aminobenzoato – EDMAB (1.0 wt.%) (Aldrich Chemical Company, Inc., Milwaukee, WI, USA) were added and the composites were mixed in a dual asymmetric centrifugal mixing system (DAC 150.1 FVZ SpeedMixer centrifuge, FlackTek Inc., Herrliberg, Germany) using three one-minute cycles at 1500 rpm. All the specimens in the present study were light-cured with a LED light unit (Radii-Cal, SDI, Victoria, Australia) using an irradiance of 650 mW/cm^2 for 40 s.

2.3. Remineralizing potential evaluation

For this part of the study, an additional group produced with Z350 resin composite (3 M ESPE, St Paul, MN, USA) was used as a commercial control. Fig. 1 shows a schematic diagram of this part of the experiment.

2.3.1. Preparation of cavities

Twenty-five extracted human molars had their roots removed at the cementoenamel junction and the crowns sectioned in the mesiodistal direction (Isomet 1000 precision saw, Buëhler, Lake Bluff, IL, USA).

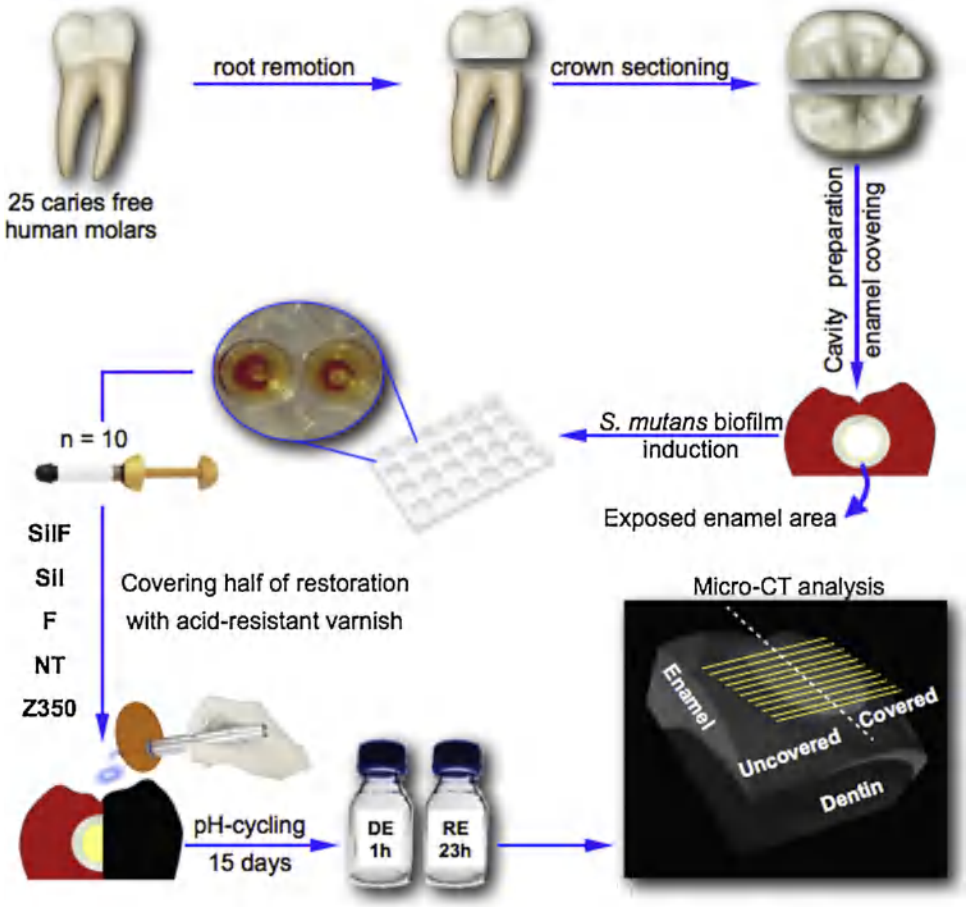

Fig. 1. Schematic diagram for remineralization potential evaluation.

Cylindrical cavities (∅ = 2 mm, deep = 1.5 mm) were prepared in the bucal and palatal surfaces of each tooth fragment, using a diamond bur (#2294, KG Sorensen, Cotia - SP - Brazil) in a high-speed hand-piece fixed in a special sample aligning device. With the exception of 2 mm around the cavities, all tooth fragments were covered with two layers of an acid-resistant varnish. Afterwards, the cavities were randomly divided into five groups (n = 10), according to the five tested composites.

2.3.2. Caries-like enamel lesions induction

Caries-like enamel lesions were created by *S. mutans* biofilm. The tooth fragments with the cavities were sterilized using ethylene oxide and placed on 24-well plates (TPP, 24 ZellkulturFestplatte F), with the surface of the cavities facing up. *S. mutans* ATCC 25175 (American Type Culture Collection, Rio de Janeiro, RJ, Brazil) was cultured in 20 ml of brain heart infusion (BHI) (Difco, Sparks, USA) broth supplemented with 2% sucrose at 37 °C in an anaerobic condition for 24 h. Afterwards, the bacterial suspension was adjusted to an optical density of 0.5 at 550 nm using a UV/Vis Spectrophotometer (Beckman Coulter DU® 530, LifeScience, San Diego, CA, USA) in accordance with the McFarland scale (Biomérieux Brazil S.A., RJ, Brazil). The suspension was diluted by 1:100. Ten µl of this suspension was added into each well containing a tooth fragment, with 2 ml of BHI broth supplemented with 2% sucrose [22]. The 24-well plates were incubated at 37 °C in an anaerobic condition for seven days. The growth medium was changed every 24 h.

2.3.3. pH-cycling

After caries-like enamel lesions production, the tooth fragments were immersed in deionized water, dried with tissue paper, and the cavities were hybridized with Adper Single Bond 2 (3 M ESPE. St Paul, MN, USA) and bulk restored with the composites. Half of each restoration and subjacent enamel were protected with an acid-resistant varnish to create a reference area and the fragments submitted to pH-cycling for 15 days: Alternate immersion in demineralizing solution (1 h): 3.0 mmol/L of $CaCl_2$, 1.8 mmol/L of KH_2PO_4, 0.1 mmol/L of lactic acid and 1% of carboxymethylcellulose, pH = 4.0, and remineralizing solution (23 h): 1.2 mmol/L of $CaCl_2$, 0.72 mmol/L of K_2HPO_4, 2.6 µmol/L of NaF and 50 mmol/L of buffer TRIS, pH = 7. Each fragment was immersed in 20 ml of each solution at 37 °C, which was changed daily.

2.3.4. Micro-CT acquisition and reconstruction procedures

After the pH-cycling, the specimens were scanned using a high energy micro-CT (Skyscan 1173, Bruker micro-CT, Kontich, Belgium). Specimens were wrapped in parafilm™ during the scanning procedures to avoid desiccation. Acquisition parameters were: 70 kV, 114 µA, detector size 2240 × 2240 pixels, 8.19 µm pixel size, 1 mm thick Al filter, 1 s exposure time, 0.5° rotation step over 360°, frame averaging of 5, random movements of 40. Scanning time was approximately 85 min for each specimen. After acquisition, cross-sections of each specimen were reconstructed using a proprietary software (NRecon, Bruker) using standardized parameters: ring artefact correction of 10, 75% beam hardening correction, no noise reducing filters and input of minimum (0) and maximum (0.15) contrast limits.

2.3.5. Evaluation of density profiles

The mineral content of the lesions was evaluated using density profiles [23]. The reconstructed stack was imported into a 3D visualization software interface (Dataviewer, Bruker) and a volume of interest (VOI), with a 2.5 mm thickness at the middle of the restoration, was selected. The selected VOI was imported to the ImageJ software (Fiji

implementation) and ten slices were selected for evaluation of density profiles. In each selected slice, two profiles of density values along a line were obtained (one at the exposed and one at the covered enamel region). The profiles were taken at each pixel starting from the enamel surface up to 250 µm deep into the enamel layer. The mineral loss parameter ΔZ was calculated for each profile (covered and exposed) for each specimen. After that, % of enamel remineralization was obtained following the formula: ΔZcovered - ΔZexposed)/ΔZcovered [24]. Negative values indicate a net mineral loss in enamel while positive values indicate net enamel remineralization [25].

2.4. Properties characterization

2.4.1. Degree of conversion (DC%)

Increments of the composites (n = 5) were inserted into a mold (0.785 mm^3) positioned onto an ATR crystal of the FT-IR spectrometer (Alpha-P/Platinum ATR Module, Bruker Optics GmbH, Ettlingen, Germany). The spectra of cured and uncured increments were recorded between 1600 and 1800 cm^{-1} with 40 scans at a resolution of 4 cm^{-1}. The DC% was calculated from the ratio between the integrated area of absorption bands of the aliphatic C═C bond (1638 cm^{-1}) to that of aromatic C═C bond (1608 cm^{-1}), used as an internal standard, using the following equation:

$$DC\% = 100x\left[1 - \frac{(aliphaticC = C)/(aromaticC = C)cured}{(aliphaticC = C)/(aromaticC = C)uncured}\right]$$

2.4.2. Flexural strength (FS)

Ten bar-shaped specimens (w = 2.0 mm, l = 10.0 mm, h = 1.0 mm), light-cured from the top and bottom sides were prepared for each composite. After storage in distilled water at 37 °C for 24 h, the bars were submitted to three-point bending test in an universal testing machine (DL 2000, EMIC, SP, Brazil) with 8.0 mm span, at a cross-head speed of 1 mm/min. The flexural strength (FS) in MPa was calculated using the following equation:

$$FS = \frac{3lF}{2wh^2}$$

where l is the span (mm) between supports, F is the failure load (N), h is the height (mm), and w is the width (mm).

2.4.3. Hardness (KHN)

Five disk-shaped specimens (d = 3.0 mm x h = 2.0 mm, n = 5) were prepared for each composite. After the top surfaces were polished with 1200, 2500 and 4000 grit SiC paper (DPU-10, Struers, Copenhagen, Denmark), five Knoop indentations (25 g / 15 s), spaced 200 µm apart were made in each disk (Micromet 5104 - Full MHT software, Buëhler, Lake Bluff, IL USA). The average of five indentations were taken as the KHN for each specimen.

2.5. Statistical analysis

The data were analyzed using the Statgraphics Centurion XVI software (STATPOINT Technologies, INC, EUA). Initially, the normal distribution of errors and the homogeneity of variances were checked by Shapiro-Wilk's test and Levene's test. Based on these preliminary analyses, the data were submitted to one-way ANOVA and Tukey's HSD post-hoc test. Intra-group comparison of lesion depth (covered X exposed sides) was performed by means of a paired T-test. The analysis were performed at a significance level of α = 0.05.

3. Results

Fig. 2 depicts a representative image of the HAp size distribution analysis showing that the HAp particles ranged from 10 to 970 nm, with a mean size of 34 nm. Fig. 3shows representative images of TEM and B.E.T. analysis. (A) Irregular sintered Si-HAp particle with several nanopores (red asterisks) within its structure. (B) Detailed view of a spherical Si particle surrounded and sintered to several irregular HAp particles. (C) B.E.T. adsorption-desorption Isotherm. The sintered Si-HAp particles presented a surface area of 18 m^2/g and a mean pore diameter of 749 Å.

Mean mineral profiles and ΔZ of enamel margins after 15 days of pH-cycling for each experimental composite are shown in Fig. 4. Z350, NT, and Sil showed no recovering of enamel mineral loss after 15 days of pH-cycling, while composites F and SilF presented substantial enamel remineralization after 15 days of pH-cycling. Fig. 5 shows the absolute values of enamel remineralization (%) after 15 days of pH-cycling. The highest remineralizing potential was presented by F, followed by SilF ($p < 0.05$). Contrarily, Z350, Sil and, NT showed further mineral loss after this cariogenic challenge, with the worst result being presented by Z350 ($p < 0.05$). Table 2 shows mean lesion depth on the covered (carious control) side and exposed (remineralized) side according to each dental composite. Only composites F and SilF demonstrated a net reduction in lesion depth, but this reduction was only statistically significant for composite F ($p < 0.05$). The deepest lesion at the exposed side was presented by Z350 ($p < 0.05$).

The results of DC%, FS and KHN are summarized in Table 3. Regarding DC%, ANOVA detected statistically significant differences among composites (p = 0.0014), with NT, Sil and F presenting the highest DC% ($p < 0.05$). SilF presented the lowest DC% ($p < 0.05$), but was not statistically different from Sil and F. With respect to FS, there was statistical significance for composites ($p < 0.05$). NT and Sil showed similar and higher flexural strength when compared to SilF and F, which were not different from each other. No statistically difference in hardness among the composites was found ($p > 0.05$).

4. Discussion

Different strategies to produce bioactive particles capable of releasing suitable levels of Ca^{2+}, PO_4^{3-} and F- for enamel remineralization have been proposed. However, most of these strategies involve sophisticated techniques for producing these particles [7,9,10,15,25]. In the present study, a simple method is presented using thermal sintering to fabricate Si-Hap nanoporous particles with the potential for enamel remineralization. The idea was based on the study of Atai et al. [26] who showed that experimental composites with thermally sintered nanoporous silica particles exhibited mechanical properties comparable to those of commercially available dental composites. The Si-HAp particles were produced with spherical silica nanoparticles and irregular hydroxyapatite nanoparticles with different sizes in order to produce nanopores capable of acting as a reservoir for NaF. The rationale to this was to allow for fluoride release without changing the architecture of these particles. The temperature of 900 °C was chose for producing the Si-HAp particles because it is suitable for sintering HAp without interfering with its structure and crystallinity as well as avoiding its decomposition. These aspects are crucial for maintaining the HAp physicomechanical properties and bioactivity [27].

The features seen in Fig. 2, where a wide range of size distribution of HAp particles can be noted, and in Fig. 3 A, where a Si-HAp nanocluster presents several nanopores inside its structure (red asterisks), might confirm the success of the protocol used to produce the Si-HAp nanoporous particles. Also, the entrapment of a spherical Si particle by several irregular HAp particles (Fig. 3B) might confirm the sintering among these particles.

The results of BET analysis (Fig. 3C) showed that Si-HAp particles reached a surface area of 18 m^2/g. Comparing this result with that of Atai et al. [26], who produced sintered silica particles with 8.4 m^2/g of surface area, it can be assumed that the higher surface area to volume ratio of Si-HAp produced here might be efficient for Ca^{2+}, PO_4^{3-} and F-releasing, which could have improved the potential for enamel

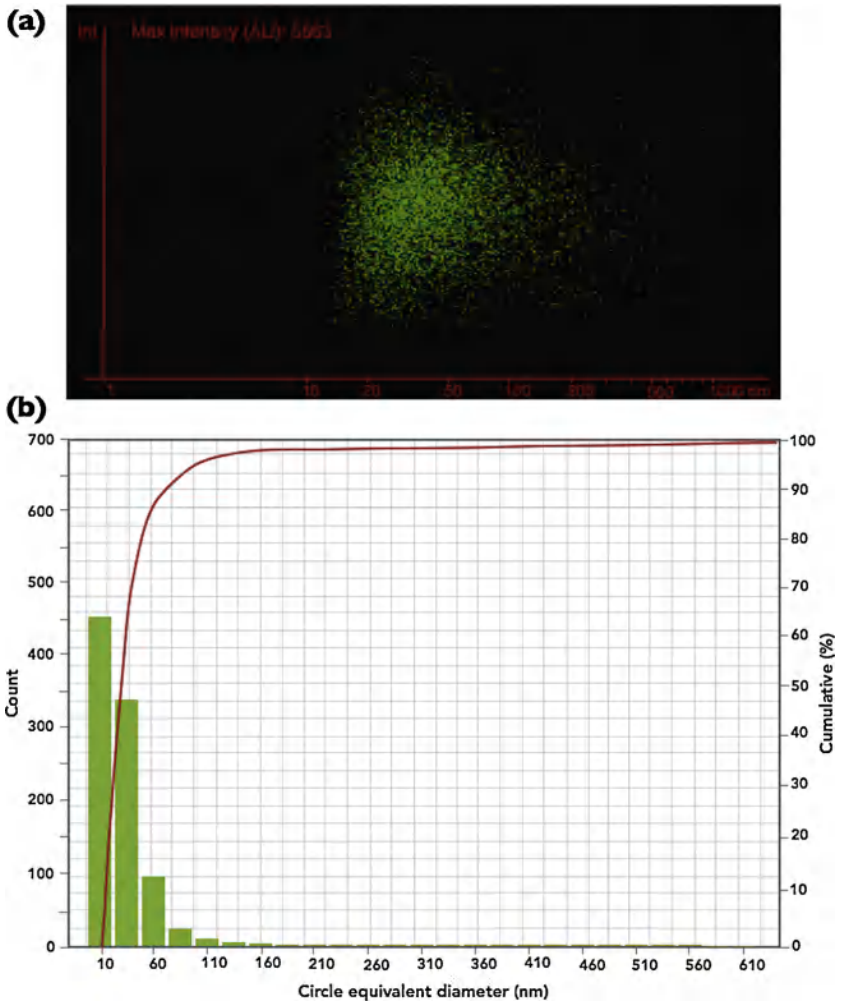

Fig. 2. Size distribution of the HAp particles determined by NanoSight LM10 system. (a) image of the HAp particles dispersed in the test medium, and (b) histogram of the circle equivalent diameter (nm) of the HAp particles.

remineralization [17,28].

Different from previous studies, in which caries-like enamel lesions were created by immersing the specimens in acidic solutions [11,24,25], the present study submitted the specimens to *S. Mutans* biofilm for seven days. Although there is no evidence about differences on caries formation produced by both methods, the first does not replicate biofilm formation, which is likely key component of clinical lesion formation [29]. This was made in attempt to simulate the caries process as closely as possible to that occurring in a clinical situation in order to correctly estimate the remineralizing potential of dental composites [14,30].

As the composites charged with NaF (F and SilF) induced remineralization of the caries-like enamel lesions (Figs. 4 and 5), the first hypothesis of the present study was accepted. When HAp comes in contact with an aqueous solution of fluorides, the negatively charged OH^- in the OH sites of its backbone are easily substituted by F-, with the consequent formation of the more stable fluoroapatite [$Ca_{10}(PO_4)_6F_2$] [31]. Moreover, pH is the driving force for this reaction [19]. Thus, one can suppose that the remineralizing mechanism presented by F and SilF was due to the loosely bound NaF, entrapped in the nanopores of Si-HAp particles (Fig. 3A), providing suitable levels of F- during pH cycling. In other words, during 1 h of immersion in the demineralizing solution at pH 4, F- release would be increased, reducing the enamel demineralization, with part of Ca^{2+} and PO_4^{3}- lost as hydroxyapatite returning to the tooth as fluoroapatite. After that, during 23 h of immersion in the mineralizing solution at pH 7, this F- would favour the remineralization, with the formation of more stable fluoroapatite on the enamel structure [14].

Although F and SilF were charged with the same amount of NaF, the first composite produced statistically higher enamel remineralization (Fig. 5/Table 2). Thus, the fluoride deposited over the surfaces of the primary HAp particles were likely entrapped by the silane layer, thereby not having a role in enamel mineralization. This is in line with the study of Xu et al., [17] who showed that silanized nanoparticles of dicalcium phosphate anhydrous (DCPA) released a lower amount of Ca^{2+}, PO_4^{3-} when compared to non-silanized DCPA. These authors claimed that this drop in ion releasing was due to the hydrophobic character of α-methacryloxypropyl-1-trimethoxysilane (α-MPS) hindering the access of water to the particles, thereby slowing their dissolution. Reinforcing this possibility, Mousa et al. [32] also showed that silanization with α-MPS interfered with ion releasing from apatite particles when immersed in acidic solutions. Based on this explanation, it is reasonable to claim that the free NaF hosted in the nanopores of Si-HAp particles played the principal role of enamel remineralization observed in the current study. The comparison of the absolute values of enamel remineralization produced by F (58.6%) and SilF (37.8%), which were statistically different (Fig. 5), reinforces the negative effect of silanization on enamel remineralization, leading to the rejection of the second hypothesis of the study.

Although NT was not capable of recovering the mineral loss of enamel, it can be observed that its value (-14.5%) was 46.9% lower than that of Z350 (−27.3%) (Fig. 5). Previous studies have shown that

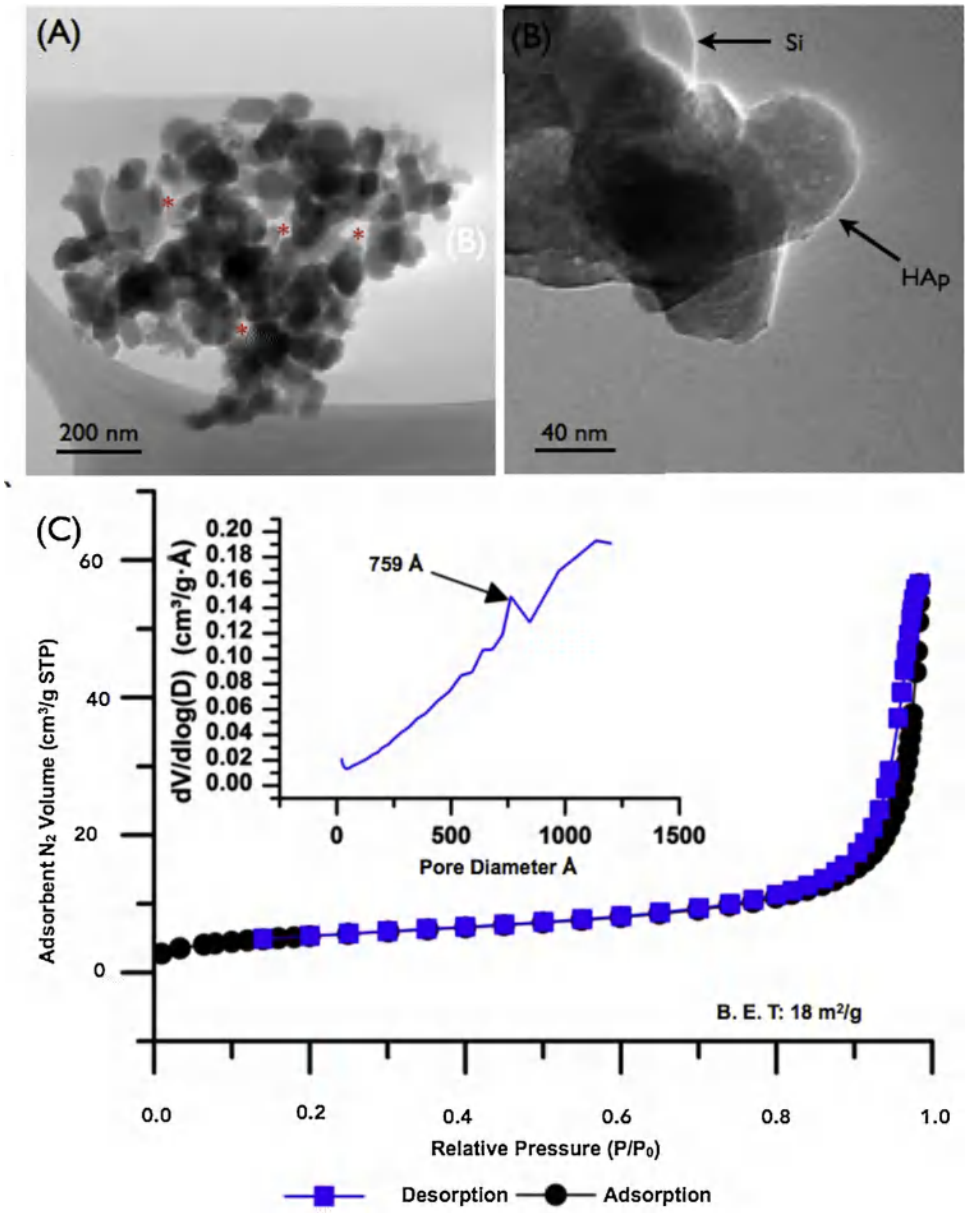

Fig. 3. Representative images of characterization of Si-HAp particles. (A) large magnification showing an irregular (800 nm) particle of Si-Hap with several pores in its interior (red asterisks). (B) low magnification showing a spherical Si particle (60 nm) surrounded and sintered to several irregular HAp particles. (C) B.E.T. adsorption-desorption Isotherm confirming a surface area of 18 m^2/g and pore diameter of 749 Å (For interpretation of the references to colour in this figure legend, the reader is referred to the web version of this article).

experimental composites with different calcium phosphate particles were capable of releasing supersaturating levels of Ca^{2+} and PO_4^{3-} and/or remineralizing caries-like enamel lesions during pH challenges [11,24,25,33,34]. Thus, it is reasonable to claim that this less mineral loss produced by NT was due to continuous Ca^{2+} and PO_4^{3-} release during pH-cycling [25]. Also, although Sil has the same composition as NT, it presented a similar behaviour to Z350, which is an inert composite. This behaviour can be explained by the silane layer hindering the release of Ca^{2+} and PO_4^{3-} by Sil, which could have negatively influenced the remineralizing potential of this composite.

When comparing the results of enamel remineralization obtained in the present study with those observed in previous publications, remarkable differences are noted. Here, the composites charged with NaF reached 58.6 ± 10.2% (F) and 37.8 ± 5.8% (SilF) of enamel remineralization, values approximately two to three fold higher than others obtained with calcium phosphate composites: 21.8 ± 3.7% [25], 14.4 ± 16.7 [24] and 23 ± 14% [11]. Apart from the differences in composition and methods used here and in these cited studies, these results clearly show that the action of F^- was crucial for the levels of enamel remineralization observed in the present study.

A high DC% is desirable for a dental composite to achieve suitable physicochemical properties [35]. In this context, 55% is suggested as the lower threshold for the composite to be applied in high-stress bearing occlusal surfaces [36,37]. Here, the DC% ranged from 56.3% to 63.84% (Table 3), values agreeing with those obtained with commercially available and experimental composites [26,38–40], which means that the protocol used to fabricate the Si-HAp particles did not negatively impact the conversion of the organic matrix of the composites. This behaviour is in line with those of other experimental resin-based materials charged with HAp particles [41,42]. On the other hand, a statistical significance was found for DC% between SilF and NT. This indicates a subtle difference in the surfaces of Si-HAp particles in SilF, produced by the entrapment of NaF onto their surfaces, which could have influenced the refraction and scattering of light during light-curing, thereby affecting the final DC% [43]. Of course, this is a speculation and needs further investigation.

The results of FS (Table 3) showed relevant aspects. NT and Sil presented statistically similar values of FS. As NT had non-silanized Si-HAp nanoporous particles, this result suggests that the micromechanical retention mechanism between the nanopores of Si-HAp

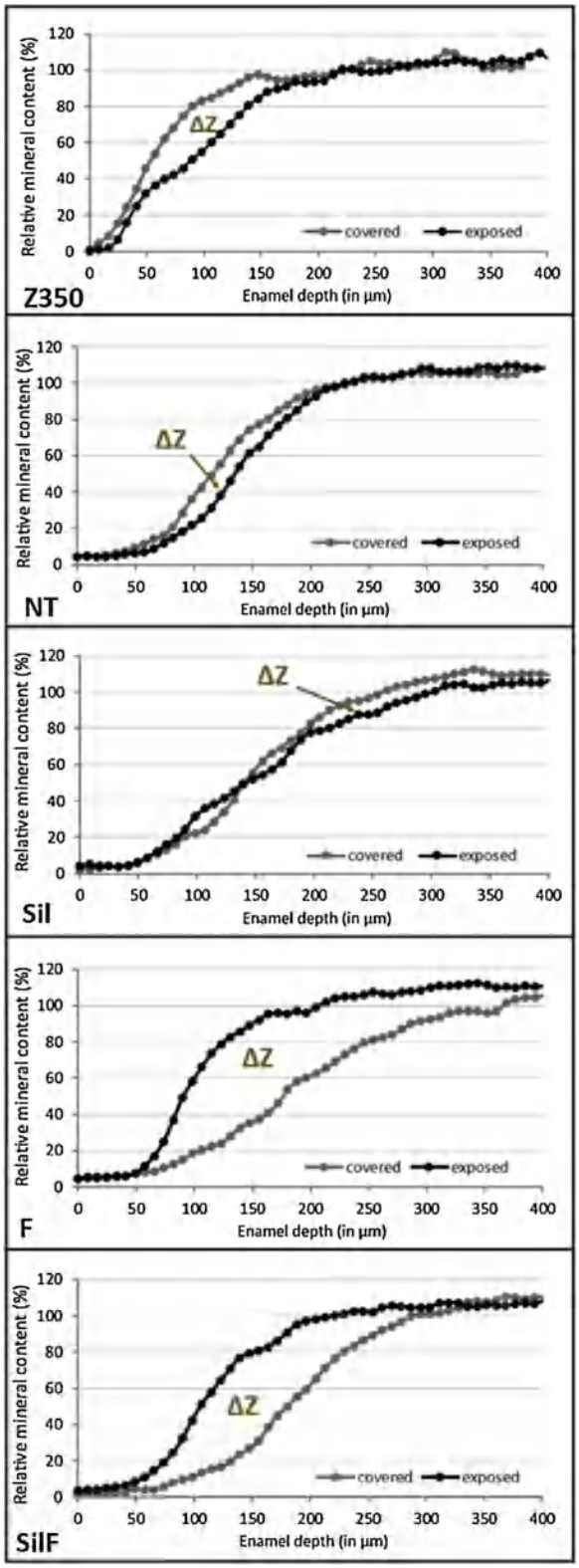

Fig. 4. Representative mineral density profiles and ΔZ of enamel margins for each experimental composite (NT, Sil, F and SilF) after 15 days of pH-cycling.

particles and the organic matrix proposed by Atai et al. [26] took place here. Also, according to Samuel et al. [44], polymerization of the organic matrix into these interconnected nanopores may create an interpenetrating rigid polymer network that provides an additional mechanical interlocking between the particles and the organic matrix. Based on this explanation, it is plausible to claim that the presence of

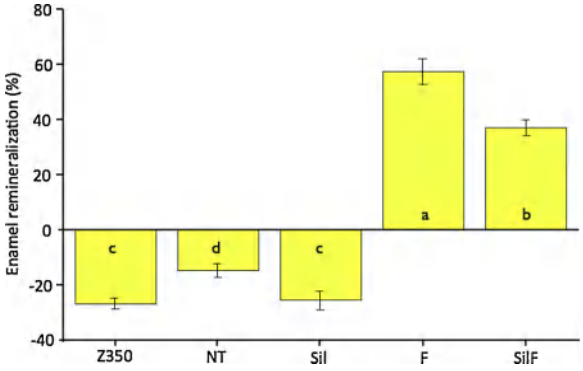

Fig. 5. Means of enamel remineralization (%) after fifteen days of pH-cycling. Bars with different letters are statistically different (Tukey´s HSD, $p < 0.05$). Error bar (standard deviation).

Table 2
Mean (± SD) of lesion depth (µm) on the covered (carious control) side and exposed (remineralized) side according to each dental composite.

Lesion depth	Covered side	Exposed side
NT	252.7 ^{a,A}(78.5)	265.1 ^{a,A}(66.9)
Sil	276.7 ^{a,A}(55.8)	293.4 ^{a,A}(73.5)
F	299.7 ^{a,A}(74.1)	190.9 ^{b,B}(60.8)
SilF	285.6 ^{a,A}(57.8)	265.5 ^{a,A}(90.5)
Z350	263.2 ^{a,A}(95.8)	345.9 ^{b,C}(84.7)

In columns, means followed by the same uppercase letter are similar (Paired t-Test, $p > 0.05$).
In rows, means followed by the same lowercase letter are similar (Tukey HSD, $p > 0.05$).

Table 3
Means (± SD) of DC%, FS (MPa), and KHN (kgf/cm^2).

Parameter	SilF	Sil	F	NT
DC	56.3 ^{B}(3.7)	61.2 ^{A,B}(1.5)	58.4 ^{A,B}(2.9)	63.8 ^{A}(0.4)
FS	40.0 ^{B}(7.8)	66.1 ^{A}(12.1)	41.1 ^{B}(4.1)	80.2 ^{A}(13.8)
KHN	32.4 ^{A}(4.2)	33.0 ^{A}(8.6)	31.4 ^{A}(4.4)	37.1 ^{A}(3.0)

In each row, means followed by different uppercase letters are statistically different (Tukey´s HSD, $p < 0.05$).

nanoporous fillers might strengthen resin composites without the necessity of chemical bonding using silanization. Contrarily, the composites charged with NaF (F and SilF) presented a similar and significantly lower FS. Most probably, this finding can be explained as the NaF hosted in the nanopores of Si-HAp particles prevented the organic matrix to enter these nanopores, thereby preventing the formation of an interpenetrating polymer network after light-curing. Moreover, the fact that silanization in SilF did not overcome this deficiency could be explained by the −OH groups on HAp surfaces having been depleted by the interaction with F^- from NaF [19], which was applied before silanization. Thus, the establishment of HAp-O-Si- bonds between Si-HAp particles and the silane [45] could have been jeopardized, thereby weakening the silanized interface.

Hardness, ranging from 31.4 to 37.1 kgf/cm^2, was the only property that showed no statistical difference among the composites (Table 3). Since hardness is dependent on the degree of conversion, organic matrix composition, type and content of fillers, and the interaction between these two phases [39,46], this result was expected.

Although this study added interesting aspects regarding the remineralizing potential of Si-HAp nanoporous particles, limitations such as the absence of ion release analysis and rechargeable capability still exist. These aspects should be addressed in future investigations.

5. Conclusion

The results of the present study showed that Si-HAp nanoporous particles charged with NaF presented an effective potential to remineralize caries-like enamel lesions produced by *S. mutans* biofilm. In some part, this ability was impacted by particle silanization. Irrespective of this, the strategy of charging Si-HAp nanoporous particles with fluorides could be an alternative for producing dental composites with improved remineralizing potential of enamel affected by caries.

Declaration of Competing Interest

The authors declare that they have no known competing financial interests or personal relationships that could have appeared to influence the work reported in this paper.

Acknowledgements

This study was financed in part by the Coordenação de Aperfeiçoamento de Pessoal de Nível Superior – Brasil (CAPES)–Finance Code 001 and by the Fundação de Amparo à Pesquisa do Estado do Rio Janeiro - FAPERJ (n° E-26/202.962/2017-BBP). The authors wish to thank the LABNANO/CBPF for the performance of the transmission electron microscopy - TEM - evaluation.

References

[1] I. Nedeljkovic, W. Teughels, J. De Munck, B. Van Meerbeek, K.L. Van Landuyt, Is secondary caries with composites a material-based problem? Dent. Mater. 31 (11) (2015) e247–77.
[2] A. Astvaldsdottir, J. Dagerhamn, J.W. van Dijken, A. Naimi-Akbar, G. Sandborgh-Englund, S. Tranaeus, M. Nilsson, Longevity of posterior resin composite restorations in adults—a systematic review, J. Dent. 43 (8) (2015) 934–954.
[3] F.F. Demarco, M.B. Correa, M.S. Cenci, R.R. Moraes, N.J. Opdam, Longevity of posterior composite restorations: not only a matter of materials, Dent. Mater. 28 (1) (2012) 87–101.
[4] D. Eltahlah, C.D. Lynch, B.L. Chadwick, I.R. Blum, N.H.F. Wilson, An update on the reasons for placement and replacement of direct restorations, J. Dent. 72 (2018) 1–7.
[5] D.C. Sarrett, Clinical challenges and the relevance of materials testing for posterior composite restorations, Dent. Mater. 21 (1) (2005) 9–20.
[6] S. Kermanshahi, J.P. Santerre, D.G. Cvitkovitch, Y. Finer, Biodegradation of resin-dentin interfaces increases bacterial microleakage, J. Dent. Res. 89 (9) (2010) 996–1001.
[7] H.H. Xu, J.L. Moreau, L. Sun, L.C. Chow, Novel CaF(2) nanocomposite with high strength and fluoride ion release, J. Dent. Res. 89 (7) (2010) 739–745.
[8] H.H. Xu, M.D. Weir, L. Sun, J.L. Moreau, S. Takagi, L.C. Chow, J.M. Antonucci, Strong nanocomposites with Ca, PO(4), and F release for caries inhibition, J. Dent. Res. 89 (1) (2010) 19–28.
[9] H.H. Xu, J.L. Moreau, L. Sun, L.C. Chow, Strength and fluoride release characteristics of a calcium fluoride based dental nanocomposite, Biomaterials 29 (32) (2008) 4261–4267.
[10] L. Sun, L.C. Chow, Preparation and properties of nano-sized calcium fluoride for dental applications, Dent. Mater. 24 (1) (2008) 111–116.
[11] Y. Alania, L.C. Natale, D. Nesadal, H. Vilela, A.C. Magalhaes, R.R. Braga, In vitro remineralization of artificial enamel caries with resin composites containing calcium phosphate particles, J. Biomed. Mater. Res. B Appl. Biomater. 107 (5) (2019) 1542–1550.
[12] P.K. Vallittu, A.R. Boccaccini, L. Hupa, D.C. Watts, Bioactive dental materials-Do they exist and what does bioactivity mean? Dent. Mater. 34 (5) (2018) 693–694.
[13] J. Abranches, L. Zeng, J.K. Kajfasz, S.R. Palmer, B. Chakraborty, Z.T. Wen, V.P. Richards, L.J. Brady, J.A. Lemos, Biology of oral Streptococci, Microbiol. Spectr 6 (5) (2018), https://doi.org/10.1128/microbiolspec.GPP3-0042-2018.
[14] J.A. Cury, B.H. de Oliveira, A.P. dos Santos, L.M. Tenuta, Are fluoride releasing dental materials clinically effective on caries control? Dent. Mater. 32 (3) (2016) 323–333.
[15] H.B. Davis, F. Gwinner, J.C. Mitchell, J.L. Ferracane, Ion release from, and fluoride recharge of a composite with a fluoride-containing bioactive glass, Dent. Mater. 30 (10) (2014) 1187–1194.
[16] I.D. Sideridou, M.M. Karabela, Effect of the amount of 3-methacyloxypropyltrimethoxysilane coupling agent on physical properties of dental resin nanocomposites, Dent. Mater. 25 (11) (2009) 1315–1324.
[17] H.H. Xu, M.D. Weir, L. Sun, Nanocomposites with Ca and PO4 release: effects of reinforcement, dicalcium phosphate particle size and silanization, Dent. Mater. 23 (12) (2007) 1482–1491.
[18] D.E. Ellis, J. Terra, O. Warschkow, M. Jiang, G.B. Gonzalez, J.S. Okasinski, M.J. Bedzyk, A.M. Rossi, J.G. Eon, A theoretical and experimental study of lead substitution in calcium hydroxyapatite, Phys. Chem. Chem. Phys. 8 (8) (2006) 967–976.
[19] M. Jimenez-Reyes, M. Solache-Rios, Sorption behavior of fluoride ions from aqueous solutions by hydroxyapatite, J. Hazard. Mater. 180 (1–3) (2010) 297–302.
[20] T.M. Chen, G.M. Brauer, Solvent effects on bonding organo-silane to silica surfaces, J. Dent. Res. 61 (12) (1982) 1439–1443.
[21] K.J. Soderholm, S.W. Shang, Molecular orientation of silane at the surface of colloidal silica, J. Dent. Res. 72 (6) (1993) 1050–1054.
[22] F. Li, M.D. Weir, J. Chen, H.H. Xu, Comparison of quaternary ammonium-containing with nano-silver-containing adhesive in antibacterial properties and cytotoxicity, Dent. Mater. 29 (4) (2013) 450–461.
[23] J. Arends, J.L. Ruben, D. Inaba, Major topics in quantitative microradiography of enamel and dentin: R parameter, mineral distribution visualization, and hyper-remineralization, Adv. Dent. Res. 11 (4) (1997) 403–414.
[24] S.E. Langhorst, J.N. O'Donnell, D. Skrtic, In vitro remineralization of enamel by polymeric amorphous calcium phosphate composite: quantitative microradiographic study, Dent. Mater. 25 (7) (2009) 884–891.
[25] M.D. Weir, L.C. Chow, H.H. Xu, Remineralization of demineralized enamel via calcium phosphate nanocomposite, J. Dent. Res. 91 (10) (2012) 979–984.
[26] M. Atai, A. Pahlavan, N. Moin, Nano-porous thermally sintered nano silica as novel fillers for dental composites, Dent. Mater. 28 (2) (2012) 133–145.
[27] A. Khoshzaban, V. Rakhshan, F. Najafi, L. Aghajanpour, S.J. Hashemian, S.H. Keshel, I. Watanabe, A. Valanezhad, T.S. Jafarzadeh Kashi, Effect of sintering temperature rise from 870 to 920 degrees C on physicomechanical and biological quality of nano-hydroxyapatite: an explorative multi-phase experimental in vitro/vivo study, Mater. Sci. Eng. C Mater. Biol. Appl. 77 (2017) 142–150.
[28] C. Chen, M.D. Weir, L. Cheng, N.J. Lin, S. Lin-Gibson, L.C. Chow, X. Zhou, H.H. Xu, Antibacterial activity and ion release of bonding agent containing amorphous calcium phosphate nanoparticles, Dent. Mater. 30 (8) (2014) 891–901.
[29] J.L. Ferracane, Models of caries formation around dental composite restorations, J. Dent. Res. 96 (4) (2017) 364–371.
[30] N.L. Brandao, M.B. Portela, L.C. Maia, A. Antonio, V. Silva, E.M.D. Silva, Model resin composites incorporating ZnO-NP: activity against S. mutans and physicochemical properties characterization, J. Appl. Oral. Sci. 26 (2018) e20170270.
[31] D.J. White, G.H. Nancollas, Physical and chemical considerations of the role of firmly and loosely bound fluoride in caries prevention, J. Dent. Res. 69 (1990) 587–594 Spec No discussion 634-6.
[32] W.F. Mousa, M. Kobayashi, Y. Kitamura, I.A. Zeineldin, T. Nakamura, Effect of silane treatment and different resin compositions on biological properties of bioactive bone cement containing apatite-wollastonite glass ceramic powder, J. Biomed. Mater. Res. 47 (3) (1999) 336–344.
[33] S.H. Dickens, G.M. Flaim, S. Takagi, Mechanical properties and biochemical activity of remineralizing resin-based Ca–PO4 cements, Dent. Mater. 19 (6) (2003) 558–566.
[34] M.A. Melo, M.D. Weir, L.K. Rodrigues, H.H. Xu, Novel calcium phosphate nanocomposite with caries-inhibition in a human in situ model, Dent. Mater. 29 (2) (2013) 231–240.
[35] J.L. Ferracane, Resin composite–state of the art, Dent. Mater. 27 (1) (2011) 29–38.
[36] N. Silikas, G. Eliades, D.C. Watts, Light intensity effects on resin-composite degree of conversion and shrinkage strain, Dent. Mater. 16 (4) (2000) 292–296.
[37] J.L. Ferracane, J.C. Mitchem, J.R. Condon, R. Todd, Wear and marginal breakdown of composites with various degrees of cure, J. Dent. Res. 76 (8) (1997) 1508–1516.
[38] J. Zorzin, E. Maier, S. Harre, T. Fey, R. Belli, U. Lohbauer, A. Petschelt, M. Taschner, Bulk-fill resin composites: polymerization properties and extended light curing, Dent. Mater. 31 (3) (2015) 293–301.
[39] E.M. da Silva, L.T. Poskus, J.G. Guimaraes, Influence of light-polymerization modes on the degree of conversion and mechanical properties of resin composites: a comparative analysis between a hybrid and a nanofilled composite, Oper. Dent. 33 (3) (2008) 287–293.
[40] E.M. da Silva, L.T. Poskus, J.G. Guimaraes, A. de Araujo Lima Barcellos, C.E. Fellows, Influence of light polymerization modes on degree of conversion and crosslink density of dental composites, J. Mater. Sci. Mater. Med. 19 (3) (2008) 1027–1032.
[41] D.M. Andrade Neto, E.V. Carvalho, E.A. Rodrigues, V.P. Feitosa, S. Sauro, G. Mele, L. Carbone, S.E. Mazzetto, L.K. Rodrigues, P.B. Fechine, Novel hydroxyapatite nanorods improve anti-caries efficacy of enamel infiltrants, Dent. Mater. 32 (6) (2016) 784–793.
[42] Y. Zhang, Y. Wang, The effect of hydroxyapatite presence on the degree of conversion and polymerization rate in a model self-etching adhesive, Dent. Mater. 28 (3) (2012) 237–244.
[43] A.S. Masotti, A.B. Onofrio, E.N. Conceicao, A.M. Spohr, UV-vis spectrophotometric direct transmittance analysis of composite resins, Dent. Mater. 23 (6) (2007) 724–730.
[44] S.P. Samuel, S. Li, I. Mukherjee, Y. Guo, A.C. Patel, G. Baran, Y. Wei, Mechanical properties of experimental dental composites containing a combination of mesoporous and nonporous spherical silica as fillers, Dent. Mater. 25 (3) (2009) 296–301.
[45] C.Y. Lung, Z. Sarfraz, A. Habib, A.S. Khan, J.P. Matinlinna, Effect of silanization of hydroxyapatite fillers on physical and mechanical properties of a bis-GMA based resin composite, J. Mech. Behav. Biomed. Mater. 54 (2016) 283–294.
[46] J.F. Besegato, E.I. Jussiani, A.C. Andrello, R.V. Fernandes, F.M. Salomao, B.L.S. Vicentin, C.C. Dezan-Garbelini, M.G. Hoeppner, Effect of light-curing protocols on the mechanical behavior of bulk-fill resin composites, J. Mech. Behav. Biomed. Mater. 90 (2019) 381–387.